ACS APPLIED MATERIALS & INTERFACES

Research Article

www.acsami.org

A Simple Evaporation Method for Large-Scale Production of Liquid Crystalline Lipid Nanoparticles with Various Internal Structures

Do-Hoon Kim,[†] Sora Lim,[‡] Jongwon Shim,[†] Ji Eun Song,[‡] Jong Soo Chang,[§] Kyeong Sik Jin,[*,∥] and Eun Chul Cho[*,‡]

[†]Amorepacific Corporation R&D Center, Yonggu-daero, Yongin, 446-729, South Korea

[‡]Department of Chemical Engineering, Hanyang University, Seoul, 133-791, South Korea

[§]Department of Agricultural Science, Korea National Open University, Seoul, 110-791, South Korea

[∥]Pohang Accelerator Laboratory, Pohang University of Science and Technology, 80 Jigokro-127-beongil, Pohang, 790-784, Korea

ABSTRACT: We present a simple and industrially accessible method of producing liquid crystalline lipid nanoparticles with various internal structures based on phytantriol, Pluronic F127, and vitamin E acetate. Bilayer vesicles were produced when an ethanolic solution dissolving the lipid components was mixed with deionized water. After the evaporation of ethanol from the aqueous mixture, vesicles were transformed into lipid-filled liquid crystalline nanoparticles with well-defined internal structures such as hexagonal lattices (mostly inverted cubic *Pn*3*m*), lined or coiled pattern (inverted hexagonal H_2), and disordered structure (inverse microemulsion, L_2), depending on the compositions. Further studies suggested that their internal structures were also affected by temperature. The internal structures were characterized from cryo-TEM and small-angle X-ray scattering results. Microcalorimetry studies were performed to investigate the degree of molecular ordering/crystallinity of lipid components within the nanostructures. From the comparative studies, we demonstrated the present method could produce the lipid nanoparticles with similar characteristics to those made from a conventional method. More importantly, the production only requires simple tools for mixing and ethanol evaporation and it is possible to produce 10 kg or so per batch of aqueous lipid nanoparticles dispersions, enabling the large-scale production of the liquid crystalline nanoparticles for various biomedical applications.

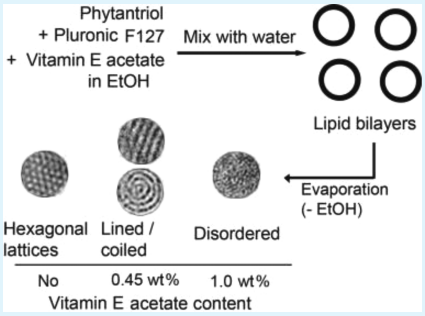

KEYWORDS: *evaporation method, lipid crystalline lipid nanoparticles, large scale synthesis, vesicles to lipid-filled nanoparticle transitions, internal structures*

1. INTRODUCTION

The field of biomedicine has great interest in liquid crystalline lipid nanoparticles with various internal structures including inverted cubic, hexagonal, and microemulsion forms.[1−5] Because they are structurally different from liposomes (aqueous dispersion of lipid bilayers) and micelles, lipid nanoparticles have the ability to carry various hydrophobic and hydrophilic drugs either inside the hydrophobic domains or water channels of the nanostructure.[6−13] These lipid nanoparticles were mostly prepared with glycerol monooleate or phytantriol (as a material for nonlamellar liquid crystalline phase) and Pluronic F-127 (as a stabilizer),[14−17] but various combinations of liquid crystalline-forming materials and stabilizers have been recently developed for the effective and uniform production of lipid nanoparticles.[18−21] As for synthetic methods, several wet-based approaches have been proposed to develop these lipid nanoparticles.[14−29] Generally, bulk nonlamellar liquid crystalline phases were mechanically chopped, homogenized, sonicated, and microfluidized in the production of nanoparticles.[14−16,19−26] Heat treatment of dispersion under high pressure were also used.[17,26,27] However, these methods may require either high mechanical/thermal energies. On the other hand, the production of the liquid crystalline nanoparticles by using a hydrotrope (i.e., ethanol),[28] from a dialysis method,[29] or by shearing process[30] suggested more efficient routes for the large scale production without using excess energies. For commercialization and various applications, it is still necessary to develop various facile and economical approaches which regulate the internal structures and functions as drug delivery carriers.

Here, we present a new simple and large-scale method to produce lipid nanoparticles with various well-defined internal nanostructures (Figure 1). In contrast to previous reports, we introduced the transformation of bilayer vesicles into lipid nanoparticles during the removal (evaporation) of one component (ethanol) in aqueous solution. The base components that we used include phytantriol, Pluronic F127, and vitamin E acetate.[16,17] When these components were mixed with a water−ethanol mixture having sufficiently high ethanol content, they formed aqueous dispersions of lipid bilayers. After

Received: July 16, 2015
Accepted: August 20, 2015
Published: August 20, 2015

DOI: 10.1021/acsami.5b06413
ACS Appl. Mater. Interfaces 2015, 7, 20438−20446

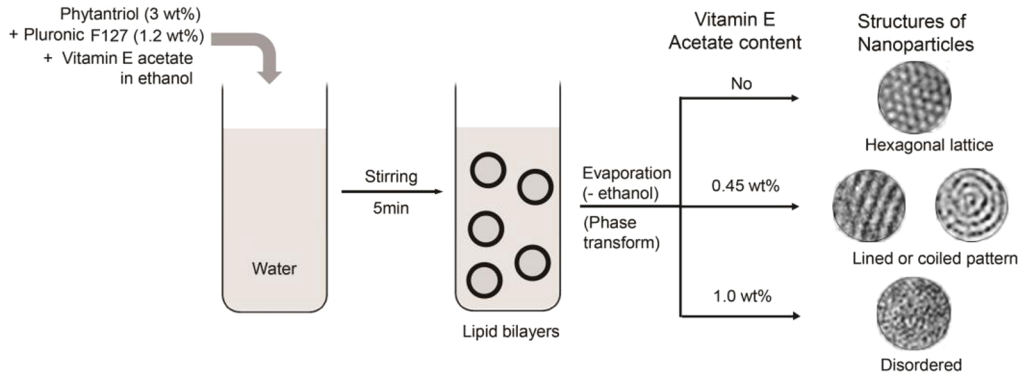

Figure 1. A schematic representing a synthetic route developed in the present work for the production of liquid crystalline lipid nanoparticles with various internal nanostructures. Lipid bilayers vesicles were produced from a simple transfer of the ethanolic mixture of Pluronic F127, phytantriol, and vitamin E acetate into deionized water under stirring. Then, a transformation of bilayer vesicles into lipid nanoparticles took place when ethanol was evaporated from a water/ethanol mixture containing the lipid components. The lipid nanoparticles had well-defined internal structures such as hexagonal lattice (mostly inverted cubic *Pn*3*m*), lined/coiled pattern (inverted hexagonal H_2), or disordered structures (inverse microemulsion, L_2), depending on the amount of vitamin E acetate.

ethanol evaporation, the bilayer vesicles restructured themselves into lipid-filled nanoparticles with well-defined internal structures: depending on the amount of vitamin E acetate, we obtained hexagonal lattices (mostly inverted cubic *Pn*3*m*), lined/coiled pattern (inverted hexagonal H_2), or disordered nanostructures (inverse microemulsion, L_2). The internal structures were also affected by temperatures. The lipid nanoparticles having different compositions varied in the degree of crystallinities (or molecular orderings among the lipid components) within the nanostructures. The sizes, internal structures, and crystallinities of the lipid nanoparticles were investigated using a dynamic light scattering, cryo-transmission electron microscope (cryo-TEM), small-angle X-ray scattering (SAXS), and microcalorimetry. In addition, the characteristics of the three lipid nanoparticles were compared with the lipid nanoparticles prepared from a conventional method.[16] Because our current method requires simple mixer and evaporator, commercially available and scalable facilities, to mix components and remove a volatile component from the aqueous solution, it can produce at least 10 kg of aqueous dispersion containing lipid nanoparticles at one time.

2. EXPERIMENTAL SECTION

2.1. Materials. Phytantriol (>96.6%) was purchased from Roche (Germany). Pluronic F127 and vitamin E acetate (>96.5%) were purchased from BASF (Germany). Ethanol and acetonitrile (HPLC, 99.9%) was purchased from Fisher Scientific (Pittsburgh, PA).

2.2. Lipid Nanoparticle Production. For the production of phytantriol-based liquid crystalline nanoparticles, 3.0 g of phytantriol and 1.2 g of Pluronic F127 were dissolved in 12.7 mL of ethanol. The ethanolic mixture was transferred into 90 mL of deionized water, and was continuously stirred with an agitator for 5 min (Daelim Electric Co, Korea). Next, most ethanol was removed using a rotary evaporator (R-200, BÜCHI, Switzerland) at 45 °C until the mass of aqueous nanoparticle dispersion became 60 g (it took approximately 1 h). After the evaporation, deionized water was added for the aqueous dispersion to be a total of 100 g, and weight concentration of phytantriol in the aqueous dispersion was 3 wt %. To produce lipid nanoparticles with different internal nanostructures, we dissolved 0.45 or 1.00 g of vitamin E acetate in the ethanol with phytantriol and F127. This ethanolic mixture was also transferred into deionized water, and the aqueous mixtures were stirred and evaporated as described above. After the evaporation, deionized water was also added for the aqueous dispersions to be a total of 100 g with lipid concentrations (phytantriol + vitamin E acetate) of 3.45 and 4 wt %, respectively.

The residual contents of ethanol in the lipid nanoparticle aqueous dispersions were determined by using a gas chromatography with flame ionization detector (GC-FID, Agilent, Santa Clara, CA). We dissolved 1 g of lipid nanoparticle aqueous dispersion in 50 mL acetonitrile. Then, we injected the solution into a column (1.0 mL/min) to carry the solution into an oven. The detection was conducted in the oven at 240 °C under nitrogen gas flow. The concentration of ethanol was quantified by comparing signals of ethanol from the GC-FID with a calibration curve in which the intensity of ethanol signals (using HPLC grade ethanol) was plotted as a function of ethanol concentration. For the three types of lipid nanoparticles, the ethanol contents were 0.2 wt % in the aqueous dispersions.

2.3. Lipid Nanoparticle Characterization. Cryo-TEM was used to investigate the morphologies of the internal structures of the lipid nanoparticles. A 7 μL fluid drop was placed on a grid with holes. Then, the grid was immersed in liquid ethane, stored in liquid nitrogen, and transferred into a Gatan model 630 cryotransfer (Gatan, Inc., Warrendale, PA) under liquid nitrogen at approximately −185 °C. A Tecnai 12 electron microscope (Philips, Eindhoven, The Netherlands) was used to observe the sample. The temperature and acceleration voltage were approximately −170 °C and 120 kV, respectively. ImageJ software was used to obtain fast Fourier transform (FTT) patterns for the TEM images. The nanoparticles' hydrodynamic diameters were measured using dynamic light scattering (Zetasizer Nano ZS90, Malvern Instrument). Microcalorimetry (VP-DSC, MicroCal, United Kingdom) was also used to monitor the thermal behavior of the lipid nanoparticles. The sample chamber was filled with 0.6 mL of aqueous nanoparticle dispersion. The reference chamber was filled with either deionized water (for lipid nanoparticles) or with a mixture of ethanol and water (for lipid vesicles). The dispersion was scanned from 5 to 70 °C at heating rate of 1 °C/min.

SAXS measurements were carried out using the 4C SAXS II beamline of the Pohang Light Source II (PLS II) with 3 GeV power at Pohang University of Science and Technology, Korea. A light source from an In-vacuum Undulator 20 (IVU20: 1.4 m length, 20 mm period) of the Pohang Light Source II storage ring was focused with a vertical focusing toroidal mirror coated with rhodium and monochromatized with a Si (111) double crystal monochromator (DCM), yielding an X-ray beam wavelength of 0.734 Å. The X-ray beam size at the sample stage was 0.1 (V) × 0.3 (H) mm^2. A two-dimensional (2D) charge-coupled detector (Mar USA, Inc.) was employed. A sample-to-detector distance (SDD) of 1.00 m for SAXS was used. The magnitude of scattering vector, $q = (4\pi/\lambda) \sin\theta$, was 0.30 $nm^{-1} < q < 6.85$ nm^{-1}, where 2θ is the scattering angle and λ is the wavelength of the X-ray beam source. The scattering angle was calibrated with silver behenate standard. We used quartz capillary with an outside diameter of 1.5 mm and wall thickness of 0.01 mm, as solution sample cells. All scattering measurements were carried out at various temperatures by using a

DOI: 10.1021/acsami.5b06413
ACS Appl. Mater. Interfaces 2015, 7, 20438−20446

FP50-HL refrigerated circulator (JULABO, Germany). The SAXS data were collected in 0.3 min. Each 2D SAXS pattern was radial averaged from the beam center and normalized to the transmitted X-ray beam intensity, which was monitored with a scintillation counter placed behind the sample. The scattering of distilled water was used as the experimental background.

3. RESULTS AND DISCUSSION

The lipid nanoparticle production first involved dissolving phytantriol and F127 in ethanol, and transferring the ethanol solution into deionized water. We used a phytantriol-to-F127 ratio of 2.5 (weight based), and ethanol concentration was 10 wt % in the aqueous dispersion. A cryo-TEM image revealed that this process resulted in the production of unilamellar bilayer vesicles with hollow interiors (Figure 2A). Next, when

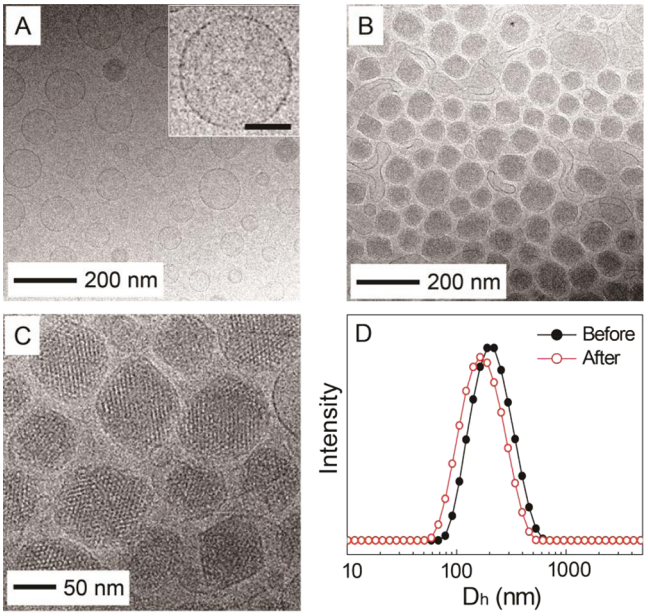

Figure 2. Cryo-TEM images of the lipid nanoparticles (A) before and (B) after the evaporation of ethanol. The lipid nanoparticles were produced with phytantriol and Pluronic F127. The concentrations of phytantriol and F127 were 3.0 and 1.2 wt %, respectively, in the aqueous dispersion. Inset in (A) is the magnified image showing bilayer vesicles (scale bar: 50 nm). (C) A magnified image of the lipid nanoparticles shown in (B). (D) Distributions of hydrodynamic diameters (D_h) before and after the evaporation of ethanol.

ethanol was removed using a rotary evaporator, the bilayer vesicles were mostly transformed into nanoparticles with lipid-filled inner structures (Figure 2B). In addition, a small number of giant vesicles with irregular shapes was also found. At high magnification (Figure 2C), the nanoparticles appeared to have a textured structure with a regular lattice. Because the entire lipid components were soluble in ethanol, the existence of ethanol in the aqueous medium may lower the interfacial free energies between the medium and the lipid components, producing the vesicular forms. While ethanol was removed, the lipid components tended to reduce the contact area with the aqueous solution. As a result of these transformations, the sizes slightly decreased. From dynamic light scattering studies (Figure 2D), the nanoparticles' hydrodynamic diameters were reduced from 197 to 179 nm after ethanol removal (Table 1), which was consistent with the trend observed in the cryo-TEM images (from 77 to 67 nm).

Table 1. Summary of Dynamic Light Scattering Results

types of lipid nanostructures			
preparation	vitamin E acetate concn (wt %)[a]	evaporation[b]	D_h (nm)
evaporation method[c]	0	before	197
		after	179
	0.45	before	205
		after	200
	1.0	before	278
		after	254
conventional method[d]	0		136
	0.45	–[e]	145
	1.0		174

[a]For all samples, the concentrations of phytantriol and F127 were 3.0 and 1.2 wt %, respectively, in the aqueous dispersion. [b]Before: before the evaporation of ethanol in the aqueous dispersions. After: after the evaporation of ethanol. [c]The method developed from the present study. [d]The method from ref 16. [e]Sonication was introduced.

Spicer et al. produced the inverted cubic liquid crystalline nanoparticles from the dilution of the mixture of ethanol and monoolein with excess F127 aqueous solution, having ethanol content of 5 wt %.[28] However, there was a possibility that the existence of a hydrotrope could weaken liquid crystal characteristics.[31] To exclude such a possibility and to produce the lipid nanoparticles with well-defined internal nanostructures sufficient for various applications, we kept evaporating ethanol (for approximately 1 h) until a trace amount remained in the aqueous dispersions. From GC-FID analysis, the amount of ethanol was only 0.2 wt % in the aqueous dispersions after the evaporation process. Most importantly, it is worth noting that the current method can produce 10 kg of lipid nanoparticles at one time, making it an industrially accessible method.

It is reported that the addition of vitamin E acetate alters the liquid crystals' internal structures.[16] We prepared the lipid nanoparticles composed of phytantriol and vitamin E acetate (Figure 3). Vitamin E acetate was codissolved in ethanol with phytantriol and F127. This ethanol mixture was then transferred into deionized water. The concentrations of vitamin E acetate used were 0.45 and 1 wt % in the aqueous dispersions, while the concentrations of the other components were kept constant. Then, vitamin E acetate/phytantriol weight ratios were 0.15 and 0.33, respectively. As in the case of the nanoparticles made without vitamin E acetate, after the evaporation, the hydrodynamic diameters of the two lipid nanoparticles also decreased (Figure 3A; from 205 to 200 nm and from 278 to 254 nm for the nanoparticle dispersion containing 0.45 and 1.0 wt % of vitamin E acetate, respectively). It is also worth noting the hydrodynamic diameters of the lipid nanoparticles were increased with increasing content of vitamin E acetate. The same trend was also observed when preparing the nanoparticles by introducing a different method[16] but with identical compositions to our lipid nanoparticles (Table 1).

We conducted cryo-TEM studies to investigate the internal nanostructure of the nanoparticles (Figures 3B–D). In the lipid nanoparticles containing 3.0 wt % of phytantriol and 0.45 wt % of vitamin E acetate, there was a lined and coiled patterns observed with cryo-TEM (Figure 3B). In the other region (Figure 3C), only the coiled pattern was observed. Analysis of several cryo-TEM images revealed a 1:1 probability of finding the two regions. The coiled and lined morphologies were not

DOI: 10.1021/acsami.5b06413
ACS Appl. Mater. Interfaces 2015, 7, 20438–20446

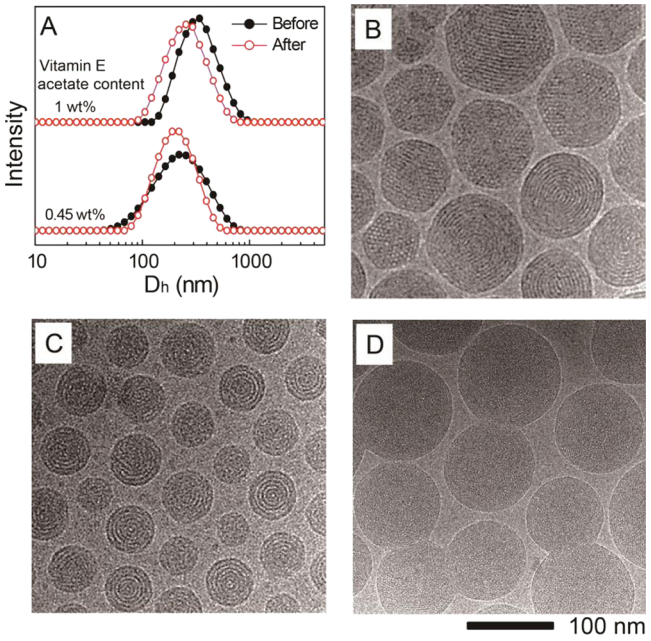

Figure 3. (A) Distributions of hydrodynamic diameters (D_h) of the lipid nanoparticles before and after the evaporation of ethanol. The lipid nanoparticles were produced with phytantriol, Pluronic F127, and vitamin E acetate. The concentrations of phytantriol and F127 were 3.0 and 1.2 wt %, respectively, in the aqueous dispersion. Vitamin E acetate concentrations were noted in the figure. Cryo-TEM images showing the different morphologies of lipid nanoparticles by varying the vitamin E acetate content in aqueous dispersions: (B and C) 0.45 and (D) 1.0 wt % (vitamin E acetate/phytantriol weight ratios were 0.15 and 0.33, respectively).

present in the nanoparticles with 3.0 wt % of phytantriol and 1.0 wt % of vitamin E acetate (Figure 3D).

Fast Fourier transform (FFT) patterns were obtained in order to investigate the internal structure of each lipid nanoparticle from the cryo-TEM images. The nanoparticles made with only phytantriol exhibited hexagonal lattices viewed from a [111] direction (Figure 4A,B), which are similar to the patterns suggesting inverted cubic structures.[17,18,22,25,26] In contrast, a ring pattern was observed in the coiled nanoparticles (3.0 wt % phytantriol and 0.45 wt % vitamin E acetate). Several literatures suggest that inverted hexagonal nanostructures generally have lined or coiled patterns,[19,24,32] while the other literature reported that they exhibit both hexagonal symmetry and curved striations.[33] Based on a phase diagram suggested by Dong et al.,[16] an inverted hexagonal phase might be expected with the weight ratio of vitamin E acetate to phytantriol was 0.15. Meanwhile, we did not observe any FFT pattern of the nanoparticles with 3.0 wt % of phytantriol and 1.0 wt % of vitamin E acetate (Figure 4E). Instead, disordered worm-like internal structures were observed (Figure 4F). Previous studies showed that the solubilization of a hydrophobic additive induces transition from cubosomes via hexosomes to micellar cubosomes and emulsified microemulsions with an internal L_2 phase.[22,25] From the results, it seems evident that the internal structures became disordered with increasing the content of vitamin E acetate.

To obtain more detailed information about the internal structures of three types of nanoparticles, we performed SAXS studies (Figure 5). The lipid nanoparticles prepared with only phytantriol showed higher-order Bragg diffraction up to the

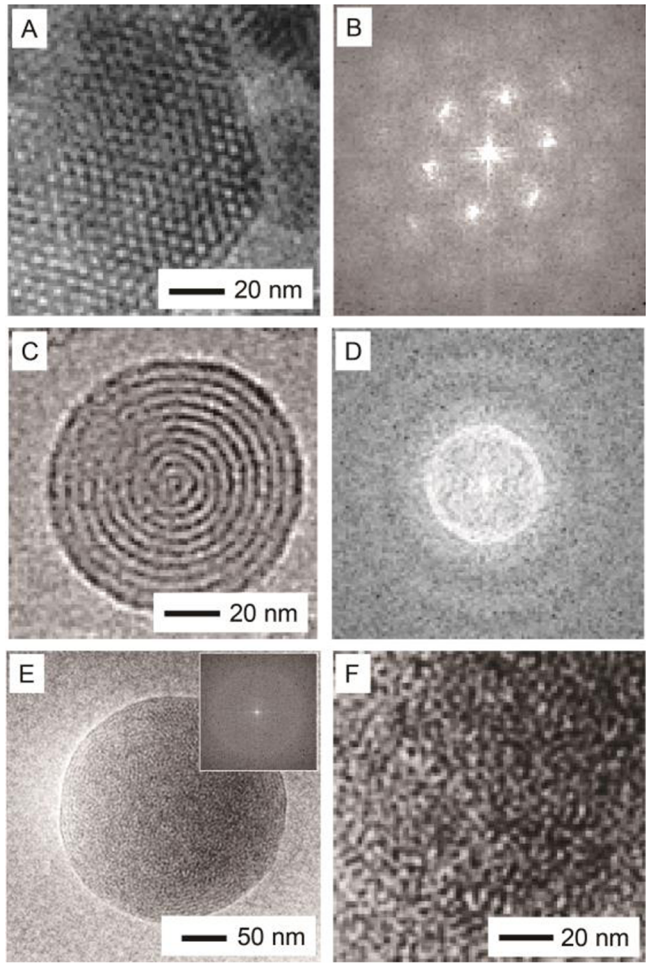

Figure 4. (A, C) Cryo-TEM images showing the internal structures and (B, D) corresponding fast Fourier Transform (FFT) patterns of the liquid crystalline lipid nanoparticles containing (A, B) 0 wt % and (C, D) 0.45 wt % vitamin E acetate in the aqueous dispersion. (E, F) High magnified cryo-TEM images of the lipid nanoparticles containing 1.0 wt % vitamin E acetate in the aqueous dispersion. Inset in E was the corresponding FFT pattern. For all the samples, the concentrations of phytantriol and F127 were 3.0 and 1.2 wt %, respectively, in the aqueous dispersion.

sixth order with a certain ratio indicated in Figure 5A, which is characterized by an inverted cubic phase with *Pn*3*m* symmetry.[25] The lattice parameter was determined to be 74.1 Å at 10 °C (Table 2). Along with the six peaks characteristics of *Pn*3*m*, a peak at 0.133 $Å^{-1}$ (marked as asterisk) was also exhibited. The peak was overlapped with the first peak in the diffraction pattern with the nanoparticles containing 3.0 wt % phytantriol and 0.45 wt % vitamin E acetate and with the ratio identified as hexagonal symmetry (H_2).[25,34] Taking the result of a recent report into account,[35] the peak corresponded primarily to the first diffraction peak from the inverted H_2 phase. The coexistence of cubic *Pn*3*m* and inverted H_2 phases might be attributable to the presence of impurities of commercial lipid phytantriol used in this study. We used the peak at 0.133 $Å^{-1}$ and the last two peaks (0.239 and 0.254 $Å^{-1}$) in the diffraction pattern to match the peak-position ratio of $1:\sqrt{3}:\sqrt{4}$ (for H_2 phase) for the determination of lattice parameters of H_2 phase. However, unfortunately, we observed a set of three reflections that did not correspond with the peak-position ratio of the H_2 phase. In the present results, it was speculated the other high-

DOI: 10.1021/acsami.5b06413
ACS Appl. Mater. Interfaces 2015, 7, 20438−20446

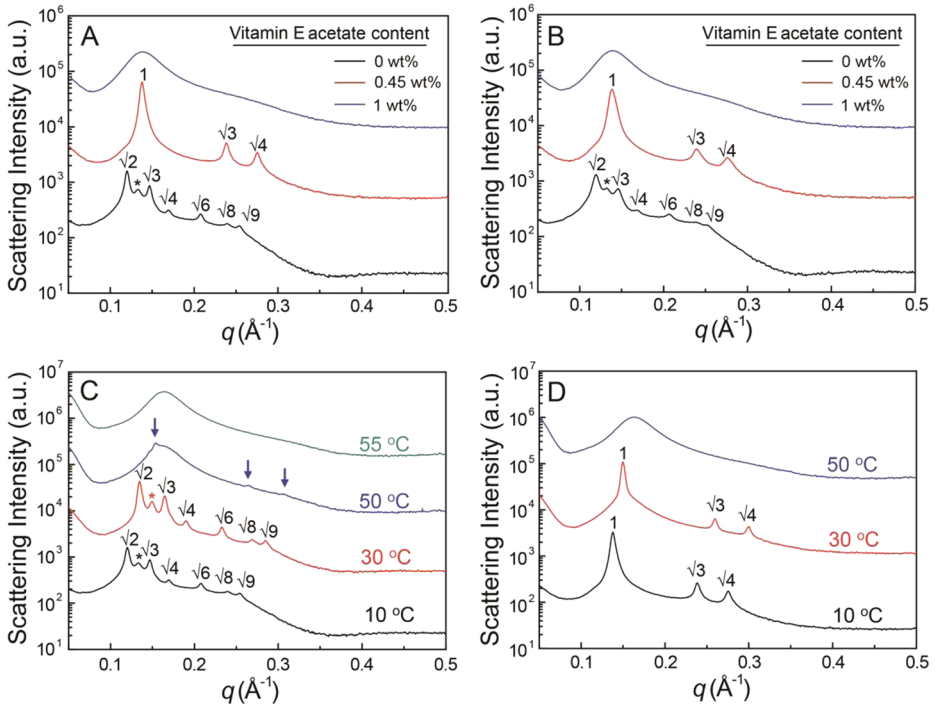

Figure 5. SAXS patterns of the liquid crystalline lipid nanoparticles prepared (A) from the present method and (B) by introducing a conventional method (ref 16). The lipid nanoparticles were produced with phytantriol, Pluronic F127, and vitamin E acetate. The concentrations of phytantriol and F127 were 3.0 and 1.2 wt %, respectively, in the aqueous dispersion. The concentrations of vitamin E acetate aqueous dispersions varied as indicated in each figure. The measurement temperature was 10 °C. (C, D) Temperature-dependent SAXS spectra for the lipid nanoparticles prepared from present method with (C) only 3.0 wt % of phytantriol and (D) 3.0 wt % of phytantriol and 0.45 wt % of vitamin E acetate. For asterisks (*) and arrows in the figures, see the text.

Table 2. Structural Parameters Obtained from the SAXS Data (Figure 5) of the Liquid Nanoparticles

preparation	vitamin E acetate concn (wt %)[a]	measurement temp (°C)	space group	lattice parameter, a (Å)
evaporation method[b]	0	10	$Pn3m$	74.1 ± 0.2
			H_2	–[c]
		30	$Pn3m$	66.0 ± 0.2
			H_2	–[c]
		50	H_2	47.4 ± 0.2
			L_2	38.9 ± 0.3[d]
		55	L_2	38.3 ± 0.3[d]
	0.45	10	H_2	52.8 ± 0.3
		30	H_2	48.5 ± 0.3
		50	L_2	38.5 ± 0.3[d]
	1.0	10	L_2	45.3 ± 0.3[d]
conventional method[e]	0	10	$Pn3m$	74.3 ± 0.3
			H_2	–[c]
	0.45	10	H_2	52.6 ± 0.3
	1.0	10	L_2	45.1 ± 0.3[d]

[a]For all the samples, the concentrations of phytantriol and F127 were 3.0 and 1.2 wt %, respectively, in the aqueous dispersion. [b]The method developed from the present study. [c]Lattice parameters were not determined due to lack of second and third peaks. See the text for the explanation. [d]The characteristic distance for the L_2 phase ($d = 2\pi/q$) from the observed single broad peak. [e]The method from ref 16.

order peaks were buried beneath the background at 10 and 30 °C, presumably due to their very low intensity. Instead, we estimated the characteristic distance (= $2\pi/q$) of 47.1 ± 0.2 Å with the peak at 0.133 $Å^{-1}$.

As explained above, the nanoparticles containing 3.0 wt % phytantriol and 0.45 wt % vitamin E acetate had the internal structure of inverted H_2 phase with a lattice parameter of 52.8 Å at 10 °C. Meanwhile, there was no characteristic peak for the lipid nanoparticles containing 3.0 wt % of phytantriol and 1.0 wt % of vitamin E acetate. The pattern was indicative of inverse microemulsion (L_2 phase) with the characteristic distance of 45.3 Å, estimated from this broad peak.

To validate the present method as an effective way for the production of lipid nanoparticles with similar quality to those obtained from conventional methods, we compared SAXS data of the lipid nanoparticles prepared from the present method with those of the nanoparticles prepared by introducing a conventional method (Figure 5B and Table 2; see Table 1 for the hydrodynamic diameters).[16] Briefly, phytantriol or mixture of phytantriol and vitamin E acetate was added to aqueous solutions containing F127 under sonication. The compositions of phytantriol, vitamin E acetate, F127, and water were identical to those of the nanoparticles prepared from the present method. Regardless of the preparation method, the space group and lattice parameter were essentially the same. Putting the cryo-TEM images and SAXS results together, we suggest the present method could not only manipulate the internal nanostructures under composition variation but also produce the lipid nanoparticles bearing similar characteristics with the nanoparticles prepared from a conventional method. In addition, the results also indicate that the presence of small amount of ethanol in the produced aqueous dispersions by applying the simple evaporation method does not affect the internal structures.

DOI: 10.1021/acsami.5b06413
ACS Appl. Mater. Interfaces 2015, 7, 20438–20446

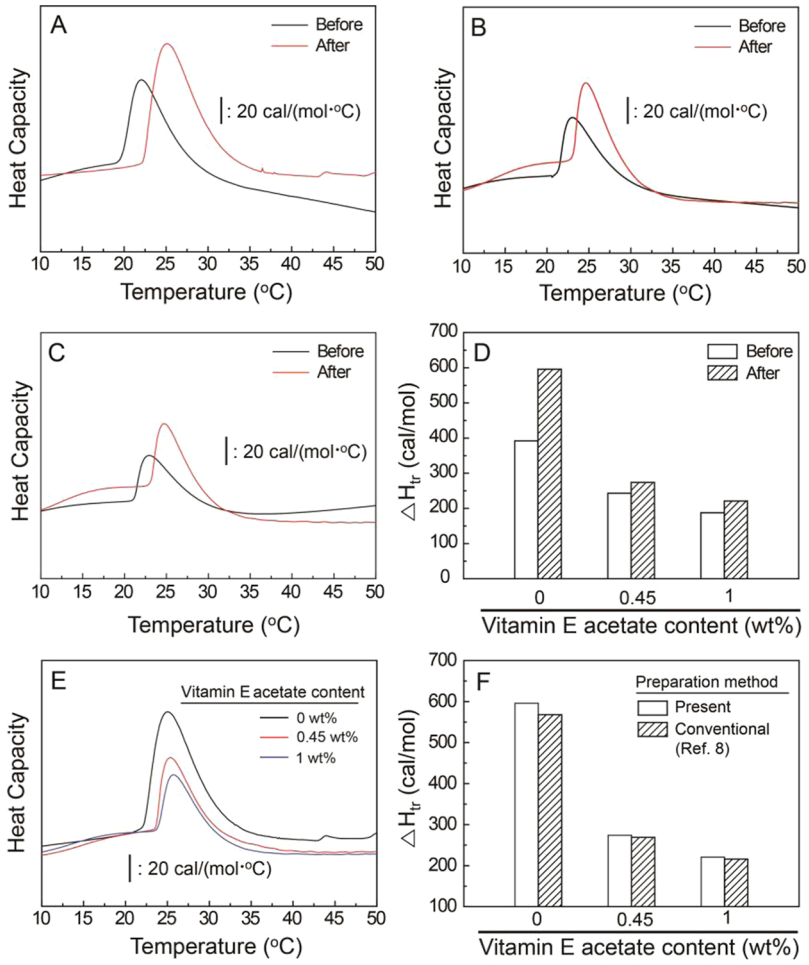

Figure 6. (A–C) Microcalorimetry thermograms of the lipid nanoparticles before and after the evaporation of ethanol. The lipid nanoparticles were produced with phytantriol (3.0 wt %), Pluronic F127 (1.2 wt %), and vitamin E acetate. The concentrations of the vitamin E acetate contents in aqueous dispersions were (A) 0, (B) 0.45, and (C) 1.0 wt %. (D) Comparisons of the transition enthalpies among the three types of lipid nanoparticles. (E) Microcalorimetry thermograms of the lipid nanoparticles prepared by introducing a conventional method (ref 16.). (F) Comparisons of enthalpies of transition between the nanoparticles prepared from the present method and those from the conventional method.

We additionally performed temperature-dependent SAXS studies with the lipid nanoparticles prepared from the present method (Figure 5C,D). For the lipid nanoparticles prepared with only phytantriol (Figure 5C), the inverted cubic *Pn*3*m* maintained at 30 °C but the peaks were shifted to higher *q* values. The lattice parameter was decreased from 74.1 Å at 10 °C to 66.0 Å at 30 °C. In addition, the peak at 0.133 $Å^{-1}$ measured at 10 °C was shifted to 0.149 $Å^{-1}$ (characteristic distance of 41.9 ± 0.2 Å) at 30 °C with increased intensity, meaning that the inverted hexagonal structure was slightly developing. At 50 °C, most peak characteristics of cubic *Pn*3*m* disappeared. Instead, a broad diffraction pattern with traces of three peaks remained (indicated as arrows): a close investigation of the three peaks revealed that they were originated from H_2 phase with a lattice parameter of 47.4 Å. Therefore, upon heating, a mixture of *Pn*3*m* and H_2 phases were transitioned to a mixture of L_2 and H_2 phases. All the peaks completely disappeared at 55 °C and the only L_2 phase existed. The similar trend was observed for the lipid nanoparticle containing 3.0 wt % of phytantriol and 0.45 wt % of vitamin E acetate (Figure 5D). The lattice parameter was decreased from 52.8 Å at 10 °C to 48.5 Å at 30 °C, and the three characteristic peaks, attributed from H_2 phase, disappeared at 50 °C. Temperature effect has been addressed by previous reports.[16,22,25,33] With increasing temperatures, inverted cubic phases transitioned to H_2 and further to L_2 phases. It was also reported that the addition of oil also induced the phase changes.[22,25] The current results were in line with the previous results.

Although the above experimental evidence proved our method produced lipid nanoparticles with similar quality to those from a conventional method, it is worth addressing that the present temperature-dependent SAXS data were a little different from the previous data reported in ref 16. In the literature, the lipid nanoparticles containing 2.7 wt % of vitamin E acetate showed an inverted cubic phase to H_2 phase transition, but a significant peak due to inversed H_2 phase still remained at 50 °C with in the nanoparticles. This is probably due to the use of impure commercial phytantriols:[36] while the literature showed only peaks characteristics of cubic *Pn*3*m*, our SAXS data suggested that the nanoparticles prepared with only phytantriol contained small portion of H_2 phase in cubic *Pn*3*m*, regardless of preparation method.

Microcalorimetry studies for the three types of lipid nanoparticles were conducted to obtain more information about the nanoparticles (Figure 6). For the nanoparticles made with only phytantriol (Figure 6A), the thermogram of the bilayer vesicles peaked at 22.0 °C before evaporation. After

DOI: 10.1021/acsami.5b06413
ACS Appl. Mater. Interfaces 2015, 7, 20438–20446

evaporation, the nanoparticles peaked at 25.0 °C. In addition, the peak intensity of heat capacity was increased after the evaporation. An analysis of the thermograms (Table 3) revealed

Table 3. Summary of Microcalorimetry Results[a]

preparation	vitamin E acetate concn (wt %)[b]	evaporation[c]	peak temp (°C)[d]	ΔH (cal/mol)[e]
evaporation method[f]	0	before	22.0	392
		after	25.0	596
	0.45	before	23.0	243
		after	24.7	274
	1.0	before	23.0	188
		after	24.7	221
conventional method[g]	0		25.0	568
	0.45	–[h]	25.3	269
	1.0		25.3	216

[a]Peak temperatures and enthalpies were obtained from the analysis of Figure 6 [b]The concentrations of phytantriol and F127 were 3.0 and 1.2 wt %, respectively, in the aqueous dispersion. [c]Before: before the evaporation of ethanol in the aqueous dispersions. After: after the evaporation of ethanol. [d]Temperatures showing the maximum peak intensities in the thermograms. [e]Enthalpy was estimated from the integration of peaks. [f]The method developed from the present study. [g]The method from ref 16. [h]Sonication was introduced.

that the enthalpies integrated from the peaks also increased by 52% (from 392 to 596 cal/mol). The same trends were observed with the nanoparticles prepared with phytantriol and vitamin E acetate (Figure 6B,C). For both nanoparticles, the peak temperatures shifted from 23 °C before evaporation to 24.7 °C after evaporation. The enthalpies of transitions were increased after the evaporation by 11% (from 243 to 274 cal/mol) and 12% (from 188 to 221 cal/mol) for the nanoparticles containing 0.45 and 1.0 wt % of vitamin E acetate, respectively. These results suggest that the change in the nanostructures from vesicles to lipid-filled nanoparticles led to an increase in the lipid nanoparticles' degree of crystallinity. In other words, the lipid nanoparticles had a higher degree of molecular order than the lipid vesicles had. This phenomenon may also result in the slight increase in the transition temperatures.

We compared the microcalorimetry results among three types of lipid nanoparticles (Figure 6D and Table 3). Each nanostructure had different degree of crystallinity. Before evaporation, the enthalpies for the transition of the bilayer vesicles containing 0.45 and 1.0 wt % vitamin E acetate decreased by 38 and 52%, respectively, when compared to those formed without vitamin E acetate. After the evaporation, the transition enthalpies of the lipid nanoparticles also decreased by 54 and 63%, respectively. These results suggest that the addition of vitamin E acetate decreases the ordered-packing among lipid components in both the bilayer vesicles and lipid nanoparticles, which may be in line with the previous literatures.[22,25] In addition, the molecular ordering of lipid components in the bilayer vesicles may greatly influence the resulting nanostructures of the lipid nanoparticles.

We also compared thermal behaviors of the lipid nanoparticles prepared from the present method with those of the nanoparticles prepared by introducing a conventional method (Figure 6E,F).[16] Similarly with Figure 6A–C, the three types of nanoparticles prepared from the conventional method showed the decreased in the peak intensities of heat capacity with increasing the vitamin E acetate contents. Comparing the thermal properties of the samples produced from the conventional method with those from the present method, peak temperatures differed by less than 0.6 °C. The enthalpies of transitions differed only by 4.9%, 1.9%, and 2.3% when the lipid nanoparticles had vitamin E concentrations of 0, 0.45, and 1.0 wt %, respectively.

It is worth discussing the origin of the transition obtained from the microcalorimetry results. The transition temperatures after the evaporation were not much different among the samples having different compositions. From the present SAXS studies for the inversed cubic and hexagonal phases, there was no indication on the structural transitions between 10 and 30 °C (Figure 5C,D), implying that the peaks observed at 24.7–25.0 °C of the lipid nanoparticles after evaporation might not be related to the phase transitions (i.e., *Pn*3*m* to H_2 or H_2 to L_2). From the literatures, the microcalorimetry generally measured order (crystal) to disorder (liquid crystal) transitions of certain lipid structures suspended in aqueous systems.[37,38] If the transition temperatures (22–23 °C) of the lipid vesicles, obtained before the evaporation, were attributed to the same reason, the transition temperatures (24.7–25.0 °C) of lipid-filled nanoparticles obtained after the evaporation might be originated from the crystal to liquid crystal transitions among the lipid components without significant changes in the liquid crystalline phases. As such, the enthalpies of transitions explained the degree of ordering among the lipid components within a certain internal structures.

4. CONCLUSIONS

Since 1996,[14] many reports have addressed liquid crystalline lipid nanoparticle structures and their ability to hold various therapeutic payloads. While these studies are very important, it is also important to establish an industrially accessible synthetic method to both increase productivity and expand the application of these nanoparticles. We produced lipid nanoparticles from bilayer vesicles through the removal (evaporation) of one component (ethanol) in aqueous solution: the method did not require excess mechanical energy or heating. Therefore, the present method can economically produce the liquid crystalline lipid nanoparticles in large quantities and with well-defined internal structures with hexagonal lattice (mostly inverted cubic), lined/coiled pattern (inverted hexagonal), and disordered forms (inverse microemulsion) depending on the compositions. We would suggest the present data are beneficial not only to those who wish to commercially use liquid crystalline lipid nanoparticles but also to those who will apply these nanostructures to various fields.

AUTHOR INFORMATION

Corresponding Authors

*E-mail: enjoe@hanyang.ac.kr.
*E-mail: jinks@postech.ac.kr.

Author Contributions

D.-H.K. and S.L. contributed equally to this work.

Notes

The authors declare no competing financial interest.
Note: After online publication, the authors became aware that a work similar to the present one was published earlier (*Langmuir* **2014**, *30*, 14452–14459).

DOI: 10.1021/acsami.5b06413
ACS Appl. Mater. Interfaces 2015, 7, 20438–20446

■ ACKNOWLEDGMENTS

We thank Amorepacific Corporation R&D Center for technical supports of this work. S.L., J.E.S., and E.C.C. are financially supported for this work by NRF (NRF-2012R1A1A1004697 and NRF-2015R1A2A2A01007003), the KETEP grant funded by the Ministry of Trade, Industry, and Energy of the Korean government (20133030000300), and National Coordinating Center for Global Cosmetics R&D (HN14C0083), South Korea.

■ REFERENCES

(1) Larsson, K. Aqueous Dispersions of Cubic Lipid-Water Phases. *Curr. Opin. Colloid Interface Sci.* **2000**, *5*, 64−69.
(2) Mulet, X.; Boyd, B. J.; Drummond, C. J. Advances in Drug Delivery and Medical Imaging Using Colloidal Lyotropic Liquid Crystalline Dispersions. *J. Colloid Interface Sci.* **2013**, *393*, 1−20.
(3) Rizwan, S. B.; Boyd, B. J.; Rades, T.; Hook, S. Bicontinuous Cubic Liquid Crystals as Sustained Delivery Systems for Peptides and Proteins. *Expert Opin. Drug Delivery* **2010**, *7*, 1133−1144.
(4) Guo, C.; Wang, J.; Cao, F.; Lee, R. J.; Zhai, G. Lyotropic Liquid Crystal Systems in Drug Delivery. *Drug Discovery Today* **2010**, *15*, 1032−1040.
(5) Lopes, L. B.; Speretta, F. F. F.; Bentley, M. V. L. B. Enhancement of Skin Penetration of Vitamin K Using Monoolein-Based Liquid Crystalline Systems. *Eur. J. Pharm. Sci.* **2007**, *32*, 209−215.
(6) Boyd, B. J. Characterisation of Drug Release from Cubosomes Using the Pressure Ultrafiltration Method. *Int. J. Pharm.* **2003**, *260*, 239−247.
(7) Boyd, B. J.; Whittaker, D. V.; Khoo, S.-M.; Davey, G. Hexosomes Formed from Glycerate Surfactants—Formulation as a Colloidal Carrier for Irinotecan. *Int. J. Pharm.* **2006**, *318*, 154−162.
(8) Swarnakar, N. K.; Jain, V.; Dubey, V.; Mishra, D.; Jain, N. K. Enhanced Oromucosal Delivery of Progesterone Via Hexosomes. *Pharm. Res.* **2007**, *24*, 2223−2230.
(9) Ahmed, A. R.; Dashevsky, A.; Bodmeier, R. Reduction in Burst Release of PLGA Microparticles by Incorporation into Cubic Phase-Forming Systems. *Eur. J. Pharm. Biopharm.* **2008**, *70*, 765−769.
(10) Nguyen, T.-H.; Hanley, T.; Porter, C. J. H.; Boyd, B. J. Nanostructured Liquid Crystalline Particles Provide Long Duration Sustained-Release Effect for a Poorly Water Soluble Drug after Oral Administration. *J. Controlled Release* **2011**, *153*, 180−186.
(11) Chen, Y.; Lu, Y.; Zhong, Y.; Wang, Q.; Wu, W.; Gao, S. Ocular Delivery of Cyclosporine A Based on Glyceryl Monooleate/Poloxamer 407 Liquid Crystalline Nanoparticles: Preparation, Characterization, In Vitro Corneal Penetration and Ocular Irritation. *J. Drug Targeting* **2012**, *20*, 856−863.
(12) Drummond, C. J.; Fong, C. Surfactant Self-Assembly Objects as Novel Drug Delivery Vehicles. *Curr. Opin. Colloid Interface Sci.* **1999**, *4*, 449−456.
(13) Sagalowicz, L.; Leser, M. E.; Watzke, H. J.; Michel, M. Monoglyceride Self-Assembly Structures as Delivery Vehicles. *Trends Food Sci. Technol.* **2006**, *17*, 204−214.
(14) Gustafsson, J.; Ljusberg-Wahren, H.; Almgren, M.; Larsson, K. Cubic Lipid-Water Phase Dispersed into Submicron Particles. *Langmuir* **1996**, *12*, 4611−4613.
(15) Gustafsson, J.; Ljusberg-Wahren, H.; Almgren, M.; Larsson, K. Submicron Particles of Reversed Lipid Phases in Water Stabilized by a Nonionic Amphiphilic Polymer. *Langmuir* **1997**, *13*, 6964−6971.
(16) Dong, Y.-D.; Larson, I.; Hanley, T.; Boyd, B. J. Bulk and Dispersed Aqueous Phase Behavior of Phytantriol: Effect of Vitamin E Acetate and F127 Polymer on Liquid Crystal Nanostructure. *Langmuir* **2006**, *22*, 9512−9518.
(17) Barauskas, J.; Johnsson, M.; Tiberg, F. Self-Assembled Lipid Superstructures: Beyond Vesicles and Liposomes. *Nano Lett.* **2005**, *5*, 1615−1619.
(18) Johnsson, M.; Barauskas, J.; Tiberg, F. Cubic Phases and Cubic Phase Dispersions in a Phospholipid-Based System. *J. Am. Chem. Soc.* **2005**, *127*, 1076−1077.
(19) Fong, C.; Weerawardena, A.; Sagnella, S. M.; Mulet, X.; Waddington, L.; Krodkiewska, I.; Drummond, C. J. Monodisperse Nonionic Phytanyl Ethylene Oxide Surfactants: High Throughput Lyotropic Liquid Crystalline Phase Determination and the Formation of Liposomes, Hexosomes and Cubosomes. *Soft Matter* **2010**, *6*, 4727−4741.
(20) Chong, J. Y. T.; Mulet, X.; Waddington, L. J.; Boyd, B. J.; Drummond, C. J. High-Throughput Discovery of Novel Steric Stabilizers for Cubic Lyotropic Liquid Crystal Nanoparticle Dispersions. *Langmuir* **2012**, *28*, 9223−9232.
(21) Chong, J. Y. T.; Mulet, X.; Keddie, D. J.; Waddington, L.; Mudie, S. T.; Boyd, B. J.; Drummond, C. J. Novel Steric Stabilizers for Lyotropic Liquid Crystalline Nanoparticles: PEGylated-Phytanyl Copolymers. *Langmuir* **2015**, *31*, 2615−2629.
(22) Yaghmur, A.; de Campo, L.; Sagalowicz, L.; Leser, M. E.; Glatter, O. Emulsified Microemulsions and Oil-Containing Liquid Crystalline Phases. *Langmuir* **2005**, *21*, 569−577.
(23) Zhai, J.; Waddington, L.; Wooster, T. J.; Aguilar, M.-I.; Boyd, B. J. Revisiting β-Casein as a Stabilizer for Lipid Liquid Crystalline Nanostructured Particles. *Langmuir* **2011**, *27*, 14757−14766.
(24) Amar-Yuli, I.; Wachtel, E.; Shoshan, E. B.; Danino, D.; Aserin, A.; Garti, N. Hexosome and Hexagonal Phases Mediated by Hydration and Polymeric Stabilizer. *Langmuir* **2007**, *23*, 3637−3645.
(25) Yaghmur, A.; de Campo, L.; Salentinig, S.; Sagalowicz, L.; Leser, M. E.; Glatter, O. Oil-Loaded Monolinolein-Based Particles with Confined Inverse Discontinuous Cubic Structure (*Fd*3*m*). *Langmuir* **2006**, *22*, 517−521.
(26) Barauskas, J.; Johnsson, M.; Joabsson, F.; Tiberg, F. Cubic Phase Nanoparticles (Cubosome): Principles for Controlling Size, Structure, and Stability. *Langmuir* **2005**, *21*, 2569−2577.
(27) Johnsson, M.; Lam, Y.; Barauskas, J.; Tiberg, F. Aqueous Phase Behavior and Dispersed Nanoparticles of Diglycerol Monooleate/Glycerol Dioleate Mixtures. *Langmuir* **2005**, *21*, 5159−5165.
(28) Spicer, P. T.; Hayden, K. L. Novel Process for Producing Cubic Liquid Crystalline Nanoparticles (Cubosomes). *Langmuir* **2001**, *17*, 5748−5756.
(29) Abraham, T.; Hato, M.; Hirai, M. Glycolipid Based Cubic Nanoparticles: Preparation and Structural Aspects. *Colloids Surf., B* **2004**, *35*, 107−117.
(30) Salentinig, S.; Yaghmur, A.; Guillot, S.; Glatter, O. Preparation of Highly Concentrated Nanostructured Dispersions of Controlled Size. *J. Colloid Interface Sci.* **2008**, *326*, 211−220.
(31) Pearson, J. T.; Smith, J. M. The Effect of Hydrotropic Salts on the Stability of Liquid Crystalline Systems. *J. Pharm. Pharmacol.* **1974**, *26*, 123−124.
(32) Fong, C.; Le, T.; Drummond, C. J. Lyotropic Liquid Crystal Engineering−Ordered Nanostructured Small Molecule Amphiphile Self-Assembly Materials by Design. *Chem. Soc. Rev.* **2012**, *41*, 1297−1322.
(33) de Campo, L.; Yaghmur, A.; Sagalowicz, L.; Leser, M. E.; Watzke, H.; Glatter, O. Reversible Phase Transitions in Emulsified Nanostructured Lipid Systems. *Langmuir* **2004**, *20*, 5254−5261.
(34) Seddon, J. M. Structure of the Inverted Hexagonal (H_{II}) Phase, and Non-lamellar Phase Transitions of Lipids. *Biochim. Biophys. Acta, Rev. Biomembr.* **1990**, *1031*, 1−69.
(35) Nilsson, C.; Barrios-Lopez, B.; Kallinen, A.; Laurinmäki, P.; Butcher, S. J.; Raki, M.; Weisell, J.; Bergström, K.; Larsen, S. W.; Østergaard, J.; Larsen, C.; Urtti, A.; Airaksinen, A. J.; Yaghmur, A. SPECT/CT Imaging of Radiolabeled Cubosomes and Hexosomes for Potential Theranostic Applications. *Biomaterials* **2013**, *34*, 8491−8503.
(36) Dong, Y.-D.; Dong, A. W.; Larson, I.; Rappolt, M.; Amenitsch, H.; Hanley, T.; Boyd, B. J. Impurities in Commercial Phytantriol Significantly Alter Its Lyotropic Liquid-Crystalline Phase Behavior. *Langmuir* **2008**, *24*, 6998−7003.

DOI: 10.1021/acsami.5b06413
ACS Appl. Mater. Interfaces 2015, 7, 20438−20446

(37) Oldfield, E.; Chapman, D. Dynamics of Lipids in Membranes: Heterogeneity and the Role of Cholesterol. *FEBS Lett.* **1972**, *23*, 285−297.
(38) Mabrey, S.; Sturtevant, J. M. Investigation of Phase Transitions of Lipids and Lipid Mixtures by High Sensitivity Differential Scanning Calorimetry. *Proc. Natl. Acad. Sci. U. S. A.* **1976**, *73*, 3862−3866.
(39) Martiel, I.; Sagalowicz, L.; Handschin, S.; Mezzenga, R. Facile Dispersion and Control of Internal Structure in Lyotropic Liquid Crystalline Particles by Auxiliary Solvent Evaporation. *Langmuir* **2014**, *30*, 14452−14459.

NOTE ADDED AFTER ASAP PUBLICATION

After ASAP publication, the authors became aware that a work similar to the present one was published earlier. The citation for that work has been added as ref 39. The corrected version was reposted on August 31, 2015.

DOI: 10.1021/acsami.5b06413
ACS Appl. Mater. Interfaces 2015, 7, 20438−20446